Quantum Time Signals in Living Beings

Brad Eckert

Abstract—We treat consciousness as a physical process occuring inside and outside of time simultaneously, per spiritual traditions and recent scientific advances. This view allows for two different dimensions of time. Quantum time emerges from consciousness as it interacts with both worlds. The relationship between the time dimensions provides a mechanism for flicker noise arising from both our biological signaling and connection to divinity. We present an algorithm for the demodulation of flicker noise. Flicker noise can have discernible information content that instruments the mind-body landscape. The demodulated signals facilitate a new class of consciousness applications. The detection and analysis of these signals has far-reaching implications for determinism, free will, heritability, and human interconnectedness.

Index Terms—Tao, flicker noise, emergent time, consciousness, QTDSP.

1 Two-Dimensional Time

According to most spiritual traditions, the consciousness of humans, animals, and all living things is a combination of the finite and the infinite, both inside and outside of material reality. Allowing more than one dimension of time theoretically supports this view of existence beyond the material world. The existence of non-local mind effects, since they hold up under serious investigation, provides a real impetus for multi-dimensional time.

Investigation of 2D time with an eye toward practical instrumentation has the potential of bearing the kind of fruit necessary to heal the schism between science and religion.

The Wheeler-DeWitt equation [1] attempts to combine mathematically the ideas of quantum mechanics and general relativity. One of its implications is the "problem of time", which is a conceptual conflict between general relativity and quantum mechanics. Quantum mechanics regards the flow of time as universal and absolute, whereas general relativity regards the flow of time as malleable and relative.

According to Wheeler-DeWitt, an observer outside of the universe doesn't experience time. Page and Wootters [2] addressed this paradox (time *seems* real enough) by treating time as an emergent phenomenon resulting from quantum entanglement. Experiments [3] on entangled particles have bolstered the theory.

There are other takes on timeless universe models. Aharonov's two state formalism of quantum mechanics has also been used [4] to propose emergence of time from a timeless unus mundus quantum-like space. Jianfeng Li provides a good overview [5] of quantum mechanical timeless consciousness.

There are two distinct types of time: emergent time, which emanates from the structure of space-time and its metrics, and a causal time, indicating the flow from the past to the future [6]. The time domains boil down to the two models of Physics, QM and GR. In the interest of a nomenclature for the masses, we call one dimension of time the quantum time domain and the other the relative time domain. So, quantum time and relative time. Relative time is the one with the arrow.

The hard problem of consciousness [7] is that of explaining the relationship between physical phenomena, such as brain processes, and experience. Experiments in non-locality [8] find that the mind extends beyond the skull. Where is the mind, inside space-time or outside? The evidence suggests it is both.

Our everyday experience is that "clock time" is the static reference frame, although it could just as well be that quantum time is the existential norm and the "clock time" universe is the special case. We take the view of quantum time observed from within the universe, with the observation being an act of quantum entanglement caused by consciousness.

1.1 Quantum Time and Consciousness

There are many examples of biological systems exploiting quantum effects. Nature would have evolved to exploit the properties of quantum time.

The physical vacuum, or classic Tao, a substrate for quantum interactions, is a natural mechanism for biological systems to have evolved to utilize. Consciousness is the interaction between the physical vacuum and biology which facilitates communication and data storage at any physical scale, from DNA to organism.

This provides an important signaling mechanism for consciousness in beings such as paramecia or slime molds, which exhibit conscious behavior but are too small for consciousness to arise from the network effects of ganglia.

One way to relate the two time dimensions is with a scale-invariant geometry that exploits the simplicity of self-similarity. As Mandelbrot [9] pointed out, relatively simple fractal mathematics underlie many complex natural phenomena. As it turns out, this exponential relationship between τ and t is a key enabler of signal transformations.

For it to be scale invariant, we use an exponential growth model for quantum time.

$$\tau \propto e^{\epsilon t} \tag{1}$$

The mechanics of signal generation can be considered in the context of quantum time. This arrangement lends itself

to information flow, utilized by nature, between the time and timeless domains.

Resonance is treated as a physical phenomenon occurring in quantum time τ. A resonant frequency in τ is equivalent to an exponential chirp in t. This dynamic emergence of time should produce small but detectable artifacts. The stream of consciousness emerges from a probabilistic field on an exponential time scale rather than time abruptly appearing from nothing.

Biological systems evolve to minimize the expenditure of energy. Resonances (field analogs of electrical and mechanical ringing) require a small energy input to keep them going, assuming a reasonably high Q. It stands to reason that biological systems would use field resonances in the physical vacuum (the exact nature of the field needs not be understood) to transmit consciousness information efficiently.

In other words, there is a theoretical basis for the notion that "It's all vibrations". The vibrations occur in quantum time, so that summing the signal artifacts from a large number of them results in a noise spectrum. Of course, nature is never simple. There could be other dimensions at play or even backward time effects providing the excitation for the resonance. Since we're only looking for artifacts, the details aren't as important as verifying the existence of the artifacts in the first place.

The signals that encode this information can be demodulated from flicker noise. The information of consciousness can then be a new media, to augment other forms of electronic media, enabling new ways of being that improve individuals and society.

2 Exponential Flicker Noise

Flicker noise (or 1/f noise), has a power spectrum proportional to $1/f^{\alpha}$, where α is between 0.7 and 1.4. It's a type of noise prevalent in many natural systems. Flicker noise [10] is seen in music, seismic data, EEG and ECG data, and electronic devices. Some of the more popular explanations for the 1/f spectrum are:

- A superposition of relaxation processes.
- Carrier mobility fluctuations through Coulomb scattering.

There are a good number of hypotheses for 1/f noise, to which we add one more:

- The superposition of exponential chirps.

An exponential swept-sine signal with constant amplitude has a power spectrum [11] that is constant-slope (on a log-log plot) at roughly -6dBm per octave, curiously similar to a flicker noise power spectrum. This is independent of "warp factor" ω.

$$Signal \propto sin(k \cdot e^{\omega t}) \tag{2}$$

2.1 Exponential White Noise

White noise has a flat power spectrum. In a white noise model of quantum time, chirps start at 0 and asymptotically approach a final frequency as quantum time merges into relative time.

$$\frac{1}{\tau} \propto (1 - e^{-\epsilon t}) \tag{3}$$

In other words, the consciousness signal emerges from a domain of infinite time. The power drops off with time at the same rate frequency increases, resulting in a flat spectrum from DC to f_0.

$$f = f_0 \cdot (1 - e^{-\epsilon t}) \tag{4}$$

$$p = p_0 \cdot e^{-\epsilon t} \tag{5}$$

f_0 would be millimeter wave (such as 60 GHz oxygen resonances) and higher. Terahertz (mostly in the 600 THz range) oscillations in tubulin [12] correlate with anesthetic potency, which opens the possibility that tubulin oscillations are carriers of consciousness information.

The chirp would mix with carrier f_0 to produce a downward chirp (assuming the signal is moving forward in time) with power dropping with frequency, which flattens out the spectrum so it's still white. That would be a more practical way to detect it due to the shortness of the time the chirp itself spends in a bandwidth that lends itself to detection. The amplitude droop may be compensated for in the input warping stage. In this scenario, white noise follows the same rules as pink noise except for the spectral bias.

This paper presents the flicker noise model, which is more practical due to its scale invariance.

2.2 Information in the Noise

Since exponential chirps are bounded in time, a single chirp has a finite existence. It corresponds to a discrete impulse in the relative time domain, or one symbol of information. The idea of consciousness as time quanta may be useful here. The act of being is a stream of consciousness that has corresponding streams of pulse-coded information, a kind of informational counterpart to DNA. The impulse stream may be decoded for its information content. The existence of an impulse stream itself is valuable, regardless of our initial ability to decode it, because useful information can be mined from its distribution of ω values.

Consciousness quanta have a foundation in Penrose and Hameroff's "Orch OR Theory" [13]. In objective reduction, the divergence of quantum superposition in the underlying structure of the universe builds to the point of collapse, or objective reduction of the quantum state. Each collapse is a moment of conscious experience. In "Orch OR", EEG is a macro view of these moments. EEG has both a flicker noise spectrum and frequency peaks that correspond to "Orch OR" collapse. There is already much scientific data (such as EEG and ECG studies) in the public domain, ready to analyze. The experimental costs are low: mostly computer hardware.

Overlapping chirps can be re-sampled and self-correlated to construct a relative time domain signal for one or a multiplicity of ω values. A sweep of ω can be used to construct a "warp spectrum" (for example, on a computer display), useful for finding quantum-time signals. This would be analogous to waterfall-style spectral analysis, with frequency replaced by warp factor.

To establish a notation and unit of measurement for the exponent of the chirp frequency, let the "warp factor" ω be in units of e, the mathematical constant derived by Leonhard Euler in the 1720s, per unit time. The pronunciation may be "e's per second" for e/s, for example. We propose "len" for the unit name of e/s, after Leonhard. Some scale factors to other units: 0.69 lens is one octave per second, 2.3 lens is one order per second, and 0.48 lens is one golden mean ($\Phi = 1.618 : 1$) per second. Note that a len is very close to twice the Golden Ratio, so one must be careful when making assumptions about Golden Ratio relationships in nature.

2.3 Spiral Conceptual Model

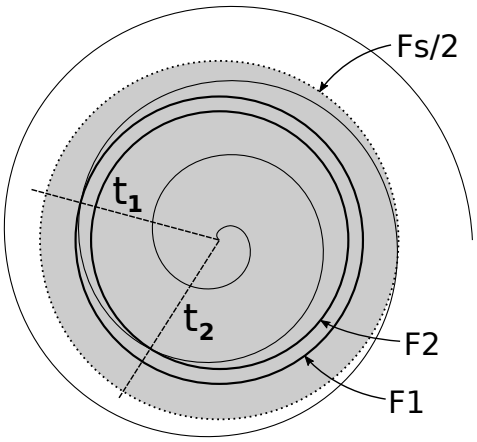

Fig. 1. Log polar plot of exponential chirp

Resonant signals in the quantum time domain can be remapped to relative time and demodulated by correlating a time series of fast exponential chirp transforms, allowing analysis and data mining using modern data processing technologies such as AI-based pattern recognition.

The correlation effect can be visualized as a spinning logarithmic spiral illuminated by a strobe light. When the strobe frequency matches the rate constant of the spiral(s), it appears to be standing still. Otherwise, it's a blur.

The relationship between quantum time and relative time can be thought of as a 2D plot in log-polar format. Log-polar format renders a logarithmic spiral as a linear (Archimedean) spiral. The spiral's radius is $\rho = k\theta$, where k is a rate constant. ρ can represent either time or frequency by flipping the sign of k. For purposes of signal processing, let ρ represent log frequency and θ relative time.

Log-polar mapping has proven useful in machine vision [14] because it approximates the primate visual map [15]. Humans are visual thinkers, so their waking consciousness should map onto the log-polar structure of quantum time signaling.

Fig. 1 plots an exponential chirp in log-polar format. A line can be drawn outward from the center of the spiral, crossing it at multiple points. The line rotates clockwise (in the case of downward chirp) at a step size (from t_1 to t_2) corresponding to the oversampling rate. For example, if the oversampling rate is 36 (each input value is used 36 times), the step size is $10°$. Each angular sweep of the unit circle

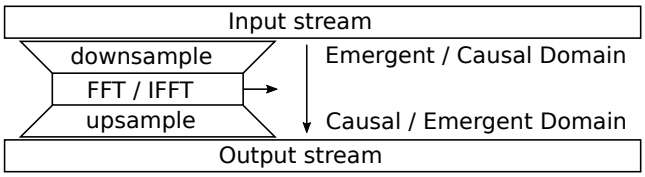

Fig. 2. Inter-domain data flow

(beginning and ending at line t_1 or t_2) represents the input to a version of the Mellin transform called the "Exponential Chirp Transform" (ECT) [14], which is basically a FFT with time-warped input.

The transform's frequency domain output is along line t_1 or t_2 from approximately ρ = 0 to Fs/2, where Fs/2 (the Nyquist frequency) is shown by the dashed circle. The radius of the circle represents the approximate bandwidth of the system. Not all of the circle is used: Anti-aliasing cuts off before Fs/2, while signal near the center is too spread out to be useful.

The ECT time-warps the chirp signal, which represents a single "quantum tone". In the $360°$ sweep at line t_1, the chirp is time-warped to a tone F1 in relative time. A time $t_2 - t_1$ later, at line t_2, it's time-warped to a tone of frequency F2. All time warping is exponential. Note that "exponential time warping" is different from dynamic time warping, a popular means of pattern-matching mostly linear signals.

A convenient side effect of time warping is to transform interference (periodic signals) into wideband noise. The usual frequency peaks of EEG and HRV are thus discarded.

Quantum time, being logarithmic, has the property of frequency going as $-\tau$ rather than $1/t$. To change between time and frequency, just flip the sign of the exponent. Tones are mirror images of time. Signal processing is more convenient in terms of frequency, so that is the focus of this paper.

2.4 Quantum Time DSP

The basic data flow of signal conversion from one time domain to another ($\tau \leftrightarrow t$) is shown in Fig. 2. The conversion algorithm slides along the input and output data streams, forward in time. Data is processed in overlapping chunks. In other words, after a block of processing, the sliding part of Fig. 2 shifts slightly to the right. In proportion to the amount of shift, new input stream is exposed and new output stream is completed. The I/O streams are low-bandwidth compared to the compute-intensive processing block.

There are two use cases: demodulation and modulation. For demodulation ($\tau \rightarrow t$), the input stream is in the quantum time domain and the output stream is in the relative time domain. The downsampler decimates the input by 1:m, where decimation factor m is exponentially swept upward from or downward to 1.0. The "warp factor" is the growth rate in m. The input stream consists of real numbers. The FFT performs a real-to-complex FFT to produce a warped spectrum which is treated as a time-domain envelope of magnitude and phase information. To un-warp the spectrum, the upsampler interpolates it by 1:m where decimation factor m is exponentially swept upward to or

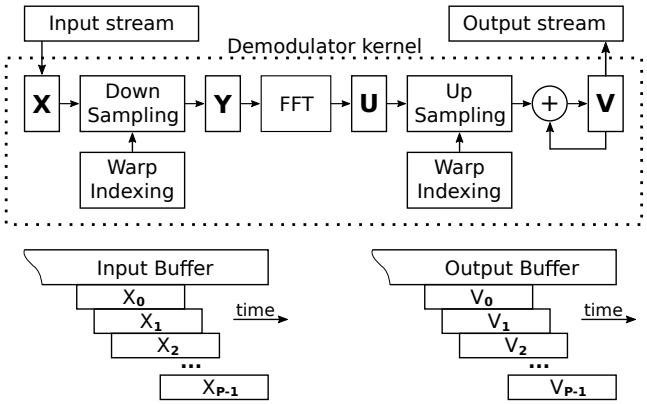

Fig. 3. Demodulation data flow

TABLE 1
Memory regions X, Y, U, and V in Fig. 3 are working buffers. For a 1k RFFT computed in place, the total is 11kB:

Buffer	Size	Bytes	Usage
X	2048 x 16	4k	Input buffer
Y/U	1024 x 24	3k	FFT working buffer
V	512 x 64	4k	Output buffer

downward from 1.0. The output stream consists of vectors that are many accumulations of overlapped upsampler results.

For modulation $(t \rightarrow \tau)$, the input stream is in the relative time domain and the output stream is in the quantum time domain. The downsampler decimates the input by 1:m, where decimation factor m is exponentially swept upward from or downward to 1.0 and the resulting spectrum ranges from about N/5 to N/2. The "warp factor" is the growth rate in m. The input stream consists of complex numbers. The IFFT performs a complex-to-real IFFT to produce a warped time domain envelope. To un-warp the it, the upsampler interpolates it by 1:m where decimation factor m is exponentially swept upward to or downward from 1.0. The output stream consists of many accumulations of overlapped upsampler results.

The usual use case is demodulation. Modulation could be for testing, reconstruction or extrapolation of a signal, or modulation of an energy source for yet unknown applications.

3 QT Demodulation

Multiple demodulator instances can be placed in an FPGA or ASIC to demodulate a large number of ω values in parallel. This would be used in spectral analysis, for finding signals; and deep data mining, for analyzing weak signals. Due to the low I/O bandwidth, the algorithm lends itself to parallelism without the complexity of high-speed signaling or memory management. A low-cost ASIC would be feasible for consumer applications.

The mathematics of signal conversion, besides FFT, is College Algebra. The algorithm can be coded by a typical programmer or engineer with some help from the following derivations.

TABLE 2
High values of M/N are undesirable because of excess processing time and memory usage. The point of diminishing returns for M/N is between 2 and 4.

M/N	$Max\|R\|$	$y_{max} : y_{min}$
2	1.256	3.51:1
4	2.337	10.35:1
8	4.229	68.66:1

3.1 Downsampling

The downsampling process of Fig. 3 translates the sample pitch of X to the sample pitch of Y using an exponential sweep. In the industry, this is known as exponential time-warping.

An exponential chirp sweeps from f_0 to f_1 in a time T. M points of X get mapped onto N points of Y, where $M > N$. Let R be a scaled version of ω for use in the exponential warp and α the X input sample rate in samples per second. Given a particular R and N, M and ω may be calculated. Let $\epsilon = (f_1/f_0)^{1/T}$. The frequency with respect to time is:

$$f = f_0 \cdot e^{\epsilon t} \tag{6}$$

3.1.1 Math

The period of the incoming chirp changes exponentially with index n of $X[n]$. Let $y = e^{|R|/N}$ be the pitch that accumulates along X. It has units of "e's per sample". As a scale factor, let $\omega = \frac{\alpha R}{N}$, in units of "e's per second" e/s. M is the number of input samples warping onto N points.

$$M = N \cdot \frac{-y \cdot ln\,(N(1-y)+1)}{|R|} \tag{7}$$

An upper limit of 2 for M/N is reasonable from both a mathematical and hardware standpoint. For example, if M is constrained to 2N, N=1024, and α = 10000 samples/second, then $|\omega|$ ranges between 0 and 12.26 e/s. When fixed-sized memories are used, smaller N allows for larger M/N, larger R, and higher ω per input sample rate.

Re-sampling is done on N points (of Y) at a time where the respective indices of X and Y are δ and i. The time span is from 0 to i/N where i sweeps from 0 to N-1 and N is the number of samples. Let λ be the sample pitch of X. It will increase or decrease exponentially and should have a minimum value of 1.0, but allowed a minimum value of less than one to allow for rounding error.

This causes a chirp of matching R to be re-sampled to the upper frequency (either f_0 or f_1 depending on the sign of R). Given output index i, input sample index $\delta(i)$ is the accumulated sum of $\lambda(i)$ when λ starts at 1.0 and increases exponentially or starts at e^{-R} and decreases exponentially. The exponential sweep can be implemented with a multiplier. For each step:

$$\lambda = \lambda + (\lambda \cdot \Lambda) \tag{8}$$

The initial value of λ is e^{-R} when $R < 0$; otherwise, it's 1. The "repeated multiply" approach to exponential sweep is nearly base e, but it needs a small correction factor to hit e. Setting $e^R = (1+\Lambda)^N$,

$$\Lambda = e^{R/N} - 1 \tag{9}$$

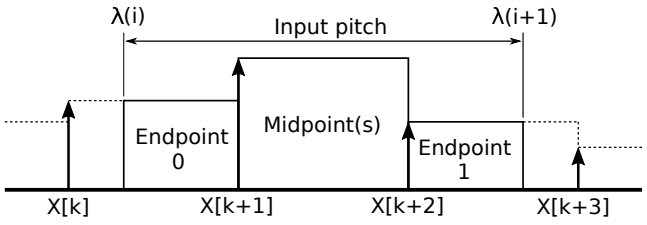

Fig. 4. Sum of X_δ for downsampling

As a sanity check, a downward-chirping sine wave was generated using a phase angle proportional to $e^{n \cdot R/N} - 1$ with index n starting from 0. Λ was set to $e^{R/N} - 1$. A 512-point FFT (with Hann window) was performed on the de-chirped wave to produce the expected narrow peak.

Verification of an exponential sweep built around a 27x26 multiplier used R=1.6 and N=8192. For upward sweep starting at 1.0, Λ was $26846167/2^{37}$ according to Eq. 9. The accumulated Λ was tracked and compared to the expected value from Eq. 7. The accumulated error after 8192 steps was less than 0.001 of an X sample pitch, so more than an order of magnitude better than necessary. Rounding was the source of error. Adding 1 to the LSB of Λ lowered it to below 0.00025. Downward sweep starting at $e^{1.6}$ had much less error. Λ was $-26840924/2^{37}$ and error peaked at 50 PPM.

3.1.2 Interpolation

The i index is stepped from 0 to N-1, where N is a power of 2 (although it doesn't have to be) for the convenience of the FFT. $\delta(i)$ sweeps non-linearly from 0 to M. For each X, its index δ is the running sum of λ. For each Y point, the downsampler averages one or more X points.

There are two ways to do handle downsampling: Linear interpolation of the output of a variable frequency low pass filter, and summation of λ input samples.

The most common downsampling method is the low pass filter whose output is sampled less often than its input rate. This method attenuates alias frequencies before they make it to the output. Anti-aliasing is good to have, but not essential in this case. Since the alias of an exponential chirp is no longer a pure exponential chirp (it's a linear combination of factors), it will show up in the data stream as wideband noise rather than narrowband interference. A low pass filter might not be needed. The computing resourced for the filter aren't cheap. However, a filter would improve SNR. Such a filter must have a linear phase response. A neat trick to use with IIR filters is forward-backward filtering, which zeros the phase shift. The endpoints of the filtered X are allowed some slop, as the Hann window will lop them off anyway.

The non-filter approach is to simply sum λ input samples of X. Some fractional arithmetic is required to handle partial contributions. Fig. 4 illustrates a simple interpolation that adds two fractional endpoints to 0 or more midpoints for downsampling. k is the integer part of δ.

In either case, the output of the downsampler could be scaled by $s = \sqrt{1/\lambda}$ to flatten the noise floor. The Central Limit Theorem reduces noise by the square root of the number of samples in a sum. On the other hand, one might expect energy conservation to cause the amplitude of the incoming signal to fall off with time spreading. So, the scaling should be optional. Another instance of exponential sweep, with $\Lambda_s = -\Lambda/2$ and $s_0 = e^{R/2N}$, can produce this scale factor rather easily.

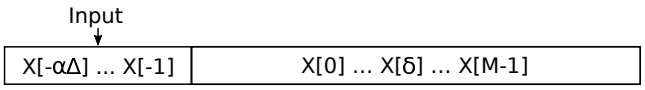

Fig. 5. X buffer usage

Oversampling would normally use a sliding window on a circular buffer sized as a power of two to allow pointer wrapping by bitwise-and. Fig. 5 shows the memory layout of X. After a block of processing, $\alpha\Delta$ input samples are concatenated to X and the index of X_0 is offset by $\alpha\Delta$, where Δ is the time interval of the blocks.

3.2 FFT

After X is time warped into Y, Y is processed by a Fast Fourier Transform and converted to data set U containing N/2 frequency bins. Y and U may share the same physical memory if the FFT is performed in place.

Polar format is preferred for the output of the FFT, for the benefit of the upsampler. A Hann window $w(n)$ is applied to Y before performing the FFT.

$$w(n) = \frac{1}{2}\left(1 - cos\left(\frac{2\pi n}{N-1}\right)\right) \tag{10}$$

The reference VHDL implementation uses a pipelined CORDIC to perform the FFT. It also applies a Hann window to Y, converts to polar output, and is shared with the correlator to perform polar to rectangular conversions.

A DIT FFT is the usual choice for RFFT since bit reversal is easier at the input. With an RFFT, you get twice the outputs given real-only input. Adjacent input samples are grouped as pairs, with even samples as real and odd samples as imaginary components of the complex input points. After a CFFT is performed, a separation step doubles the output size. Our experience is that the precision of the separation step degrades with small N (maybe we did it wrong), so a simple CFFT (with zeroed imaginary part) may be preferable in cases of small N.

An FFT can be converted to IFFT somewhat trivially, so the same hardware can support either modulation or demodulation.

3.3 Upsampling

U is upsampled to form time-domain signal V. Let ϵ and j be the respective indices of U and V. For every index ϵ of U, the corresponding frequency can be normalized to Fs/2. Letting τ be the absolute time at X_0,

$$f = \frac{\epsilon \cdot \frac{Fs}{2}}{\frac{N}{2}} = \frac{Fs}{2} \cdot e^{\omega(t-\tau)} \tag{11}$$

It's much easier to work in terms of exponents than logs, so the preferred re-mapping (another exponential time-warping) extracts $U[\epsilon]$ from a linear progression of $V[j]$. Warp indexing uses the relation:

$$\epsilon = \frac{N}{2} \cdot e^{\omega(t-\tau)} \tag{12}$$

Time t (scaled to match the output stream's sample rate) sweeps from τ in the opposite direction of R's sign, causing the exponent to start at 1 and decay downward.

Up-sampling $U[\epsilon]$ to $V[j]$ can't use the popular interpolation scheme (zero stuffing) because the interpolation factor must be irrational. Instead, partial contributions to $V[j]$ are extracted from one or two U points by interpolation.

Let Δ be the time between conversion frames, α the input sample rate, β the output sample rate, γ the input oversampling factor, and P the number of output points in period Δ.

$$P = \beta\Delta \tag{13}$$

$$\epsilon(j) = \left(\frac{N}{2} - 1\right) \cdot e^{Rj/P} \tag{14}$$

The pitch of ϵ should be 1 (when j=0) for the lowest signal loss, but it can be lowered to reduce the computational load. For this, $(\frac{N}{2} - 1) = \frac{N}{2}e^{R/P}$. So,

$$\frac{R}{P} = ln\left(1 - \frac{2}{N-2}\right) \tag{15}$$

For large N, $P \approx -0.5NR$. The sample rate relations are then:

$$\alpha \approx \frac{2\beta\gamma}{R} \tag{16}$$

$$\beta \approx \frac{\alpha R}{2\gamma} \tag{17}$$

$$\epsilon(j) \approx \left(\frac{N}{2} - 1\right) \cdot e^{-2j/N} \tag{18}$$

As a sanity check of Eq. 18, $\epsilon(j)$ starts at (N/2-1) which points to the highest frequency element of the FFT result. It decays toward 0 but will never get there. The number of elements on W memory is slightly less than N/2 to allow some I/O headroom. Due to the limited size of W memory, the lowest frequency is about $(1/e)$ of the highest frequency, leaving the lower $\approx 37\%$ of the spectrum unused.

Let H_X be the integer number of new X samples per conversion. For example, a conversion may have M = 1000 samples. An oversampling factor of 100 would give a H_X of 10. Let H_V be the number of output samples per conversion. Let k be a factor in Eq. 18 that's ≈ 2. Set the frequency shift over H_X samples equal to the $\epsilon(j)$ index.

$$N \cdot e^{-H_X \cdot R/N} = \left(\frac{N}{2} - 1\right) \cdot e^{-k \cdot H_V/N} \tag{19}$$

To make H_V an integer value, set k=2 and calculate rational H_V.

$$H_V = \frac{H_X \cdot R + ln\left(\frac{1}{2} + \frac{1}{N}\right)}{k} \tag{20}$$

Round H_V to the nearest integer and recalculate k.

$$k = \frac{H_X \cdot R + ln\left(\frac{1}{2} + \frac{1}{N}\right)}{H_V} \tag{21}$$

The exponential decay of ϵ, where $\epsilon_0 = \frac{N}{2} - 1$, can be handled by repeated multiplication. The exponential sweep needs a small correction factor to have a base of exactly e. Setting $e^{-k} = (1 + \zeta)^N$,

$$\zeta = e^{k/N} - 1 \tag{22}$$

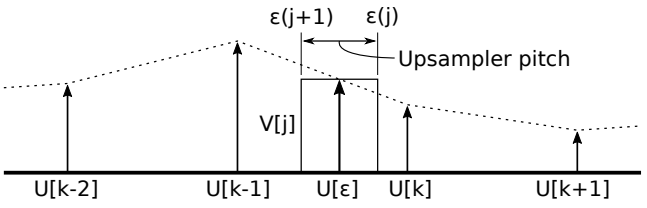

Fig. 6. Extraction of U_ϵ

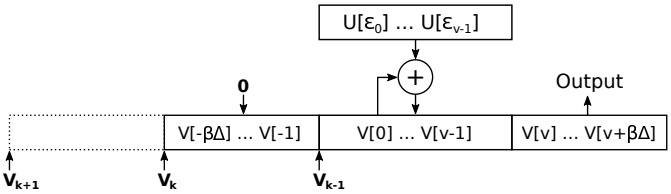

Fig. 7. Correlation of V

Since ϵ is always positive, the upchirp case of $R > 0$ needs to have its j index mirrored by using V[v-j], where v is the maximum j such as (15/32)N.

Fig. 6 shows upsampling of U to V. It uses linear interpolation to construct a curve to extract from. In this case, the upsampler input pitch is less than 1.0 samples. The height of U_ϵ is interpolated and multiplied by the pitch to get the area under the curve, to be added to V[j]. The operation is similar to the "$\lambda < 1$" case of downsampling, so the same hardware can support downsampling and upsampling.

3.4 Correlation

Warped U is added to output buffer V by the summation, staggered in time (by P samples) for each processing block. When the downsampler's R value matches the chirp rate of an incoming chirp, multiple peaks in the warped FFT output correlate in the output stream to produce a corresponding output pulse in the V stream. A more complex signal such as overlapping and/or modulated chirps will produce pulse trains and/or modulation envelopes in the V stream.

Fig. 7 shows the output correlator, another view of buffer V. The output stream flows from left to right, being initialized to 0 outside the accumulation region. After U_ϵ is added to V, the V_0 index moves $\beta\Delta$ points to the left, leaving $\beta\Delta$ newly minted output points.

Elements of V may be real (magnitudes only) or complex. Complex is used when high selectivity is required: Multiple rotating vectors will sum to zero, while vectors pointing in the same direction (chirps matching R) will correlate. Correlation through vector averaging allows the use of a much smaller FFT than scalar-only averaging. The rate of phase rotation is proportional to the FFT result frequency, so selectivity is higher at the upper end. Since the low end of the FFT result isn't used, lower selectivity there isn't a problem.

Due to the requirement that phase rotation be stationary across many FFT results for signal detection, the exponential sweeps used in downsampling and upsampling should use sufficient precision for correct tracking.

The correlator should be able to work with either vectors or real magnitudes (no phase data). This would be used in

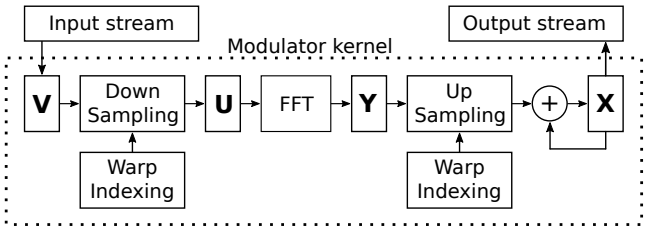

Fig. 8. Modulation data flow

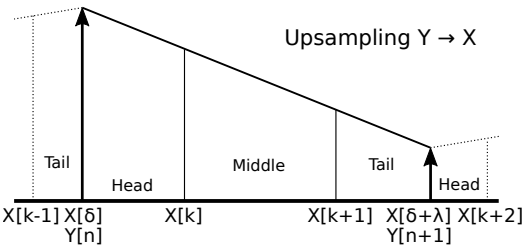

Fig. 9. Interpolation of Y for upsampling

signal search, where low selectivity is desired. The data in V, where the accumulations occur, is in rectangular format. The data coming from the upsampler is in polar format. The correlation process may use a CORDIC to perform polar-to-rectangular conversion.

4 QT MODULATION

Modulation is the reverse of demodulation. It inputs a stream of (magnitude, angle) vectors and outputs a stream of real samples. The downsample and upsample processes of modulation are the reverse of demodulaton's upsample and downsample processes respectively.

4.1 Downsampling

V is downsampled to form frequency-domain signal U. Eq. 14 relates integer index j to fractional index $\epsilon(j)$. Each point of V can be interpolated into a variable number of U points in a way that accumulates V points and spits out U points as needed.

Another view is easier to describe mathematically, but needs a logarithm. Let ϵ and j be the respective indices of U and V where $\epsilon/j < 1$. ϵ is an integer that steps downward from ϵ_0.

$$\epsilon_0 = \frac{N}{2} - 1 \tag{23}$$

Rewriting equation 14 for $j(\epsilon)$,

$$j(\epsilon) = \left(\frac{N}{2} - 1\right) ln\left(\frac{\epsilon_0}{\epsilon}\right) \tag{24}$$

The minimum ϵ is determined by the span of j. Let j range from 0 to $v - 1$ and $v = 0.469N$.

$$\epsilon(v-1) = \epsilon_0 e^{\frac{-(v-1)}{0.5N-1}} \tag{25}$$

$$\epsilon(0.469N) = \epsilon_0 e^{\frac{-(0.469N-1)}{0.5N-1}} \approx 0.391\epsilon_0 \tag{26}$$

Since ϵ is always positive, the upchirp case of $R > 0$ needs to have its j index mirrored by using V[v-j], where v is the maximum j such as 0.469N.

4.2 IFFT

The IFFT ($U \rightarrow Y$) is an Inverse Fast Fourier Transform that translates N/2 complex frequency values to N/2 complex points in the relative time domain. These may be assumed to have Hermitian symmetry, so the imaginary part of Y can be ignored. It's also possible to realize Y as N real points.

A Hann window is applied to Y after the FFT. Y is then warped and accumulated in X in a manner similar to the demodulator's correlation function.

4.3 Upsampling

The upsampling process of Fig. 8 translates the sample pitch of Y to the sample pitch of X using the reverse of the downsampling process.

Fig. 9 illustrates an interpolation scheme for recreating X from Y. The slope calculation requires a $1/\lambda$ scale factor. The expense of division can be avoided by using another instance of exponential sweep such as that described by Eq. 9.

The X points are the trapezoidal area under the curve in Fig. 9. The *Head* and *Middle* regions produce output points. The *Tail* result is carried into the next *Head*.

Summation in X is similar to the data flow of Fig. 7, but a little easier since X and Y are real (rather than complex) numbers. X memory is wider than with demodulation to handle accumulation in memory.

5 IMPLEMENTATION

The algorithms are implemented in RTL (VHDL) for use on an FPGA or ASIC. They may also be implemented in C, but certain functions are unwieldy on typical computer hardware. For example, polar-to-rectangular and rectangular-to-polar conversion is needed for upsampling complex numbers. A simple test using GCC on a Core i7 took 1.6 μs per addition. Table lookup (or other fast approximation) could speed that up: Suppose 2x, so 800 ns. In comparison, an RTL implementation using pipelined CORDIC can perform one rotated addition every two clocks. At 100 MHz, that's 20 ns.

A GPU could possibly process multiple data streams in parallel. The streams themselves are serial, so there would be a memory bottleneck. It seems FPGA is the cost/performance winner. The RTL algorithms lend themselves to multiple on-chip instances with very little I/O. There's also a migration path to ASIC for when consciousness becomes "the new media".

The RTL uses a CORDIC-based FFT with a throughput of about 7 clocks per sample. Since the FFT dominates the processing time, downsampling and upsampling are performed when the FFT is idle. This allows single-port RAM access and sharing of the CORDIC hardware. All buffers are single-port RAM for the sake of die size. Overall throughput for a demodulator is about 12 clocks per input sample, so about 10 MSPS. The input sample rate (such as from an ADC) is that divided by the oversampling factor. For example, 100x oversampling results in an ADC sample rate of 100 kSPS.

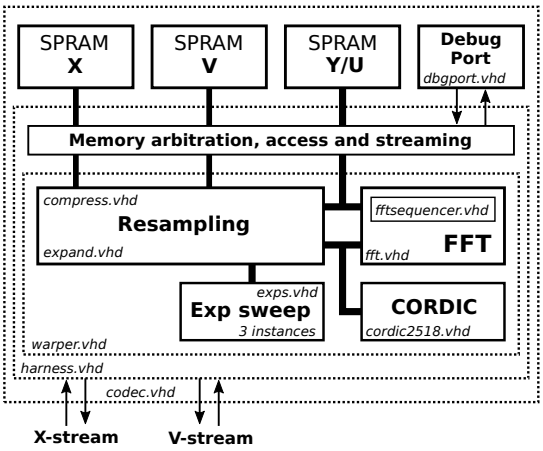

Fig. 10. RTL Block Diagram

5.1 Instrumentation

The test port uses a half-duplex byte-oriented streaming protocol to access hardware features for testing, verification, and debugging. If necessary, the I/O streams may also be handled through the test port. It uses all byte codes between 00 and FF, except for 10 to 13, which are reserved for embedded "escape sequences" and flow control. This strategy allows for XON/XOFF flow control if a UART is used as the PHY. The PHY may be a USB FIFO chip (such as FT232H), SPI, UART, JTAG, or TWI.

The test port is used with test apps to verify separate steps of the algorithm such as downsample, FFT, upsample, etc. Connection to a test PC through a 2-wire UART is sufficient for FPGA testing. The entire transform is coded in vanilla VHDL for ease of porting.

The demodulator/modulator shown in Fig. 10 uses three memory spaces to allow easier I/O access by the I/O streams and account for the difference in word widths between X and V data. The `warper` uses wide data busses on the X and V memories to facilitate correlation of outgoing data using long accumulators in either X or V memory. Incoming data is packed two points per memory word.

5.2 FPGA utilization

A complete CODEC was implemented in vanilla VHDL with a single clock domain. Free versions of synthesis tools were used to synthesize the design for use in some sample FPGAs. The clock rate is limited by the exponential sweep module, which uses a single-cycle feedback loop whose path includes a 26x27 multiplier, 4:1 mux, adder, and 3:1 mux. Those two muxes will do better on FPGAs with 6-input LUTs. Synthesis for parts with LUT6 had a 50% reduction in LUT usage compared to LUT4-only.

Quartus Prime Pro fit six cores into a 10CX105YU484I6G (20μm FPGA), with a power dissipation of about 5.8 watts at 100 MHz. A system with 6 or 8 cores could be cooled with a small fan heat sink combo.

TABLE 3
FPGA rough synthesis results. One-off distributor pricing gives a rough cost per MHz, using Digikey pricing, across the number of CODEC instances that will fit in the FPGA.

Device	Logic	DSPs	Clock	Cores	$/MHz
Artix 7	8K LUT6	40	100 MHz	12	0.16
Cyclone 10GX	38K ALM	125	100 MHz	6	0.21
LFE5	12K LE	40	39 MHz	1	0.30
PolarFire	14K LUT4	37	51 MHz	7	0.40
Cyclone 5	5K ALM	18	72 MHz	2	0.55
MAX10	13K LE	69 9x9	51 MHz	1	1.20

REFERENCES

[1] B. S. Dewitt, "Quantum theory of gravity. i. the canonical theory," *Physical Review*, vol. 160, pp. 1113–1148, 1967, doi:10.1103/PhysRev.160.1113.

[2] D. N. Page and W. K. Wootters, "Evolution without volution: Dynamics described by stationary observables," *Physical Review D*, vol. 27, no. 12, pp. 2885–2892, 1983.

[3] E. M. et al., "Time from quantum entanglement: an experimental illustration," *Physical Review A*, vol. 89, 2014, 052122.

[4] A. C. Lobo, "Time and consciousness in a quantum world," 2017.

[5] J. Li, "A timeless and spaceless quantum theory of consciousness," *NeuroQuantology*, vol. 11, pp. 431–442, 2013.

[6] O. Brunet, "Geometric time and causal time in relativistic lagrangian mechanics," 2016.

[7] D. J. Chalmers, "Facing up to the problem of consciousness," *Journal of Consciousness Studies*, vol. 2, pp. 200–219, 1995.

[8] e. a. Jeanne Achterberg, "Evidence for correlations between distant intentionality and brain function in recipients: A functional magnetic resonance imaging analysis," *Journal of Complementary and Alternative Medicine*, vol. 11, no. 6, pp. 965–971, 2005.

[9] B. Mandelbrot, *The Fractal Geometry of Nature*. W. H. Freeman and Company, 1982.

[10] E. Milotti, "1/f noise: a pedagogical review," 2002.

[11] A. N. et al, "Nonlinear system identification using exponential swept-sine signal," *IEEE Transactions on Instrumentation and Measurement*, vol. 59, no. 8, pp. 2220–2229, 2010, doi:10.1109/tim.2009.2031836.

[12] T. J. A. Craddock, "Anesthetic alterations of collective terahertz oscillations in tubulin correlate with clinical potency: Implications for anesthetic action and post-operative cognitive dysfunction," *Scientific Reports*, vol. 7, no. 1, p. 9877, 2017. [Online]. Available: https://doi.org/10.1038/s41598-017-09992-7

[13] S. Hameroff, "Consciousness in the universe: a review of the 'orch or' theory," *Physics of Life Reviews*, vol. 11, 2013.

[14] G. Bonmassar and E. L. Schwartz, "Space-variant fourier analysis: the exponential chirp transform," *IEEE Transactions on Pattern Analysis and Machine Intelligence*, vol. 19, pp. 1080–1089, 1997, DOI:10.1109/34.625108.

[15] E. L. Schwartz, "Cortical anatomy, size invariance, and spatial frequency analysis," *Perception*, vol. 10, pp. 455–469, 1981.